J. Membrane Biol. 91, 129–146 (1986)

The Journal of
Membrane Biology
© Springer-Verlag New York Inc. 1986

Characterization of the Band 3 Substrate Site in Human Red Cell Ghosts by NDS-TEMPO, a Disulfonatostilbene Spin Probe: The Function of Protons in NDS-TEMPO and Substrate-Anion Binding in Relation to Anion Transport

E. Kaufmann, G. Eberl, and K.F. Schnell
Institute of Physiology, University of Regensburg, D-8400 Regensburg, Federal Republic of Germany

Summary. NDS-TEMPO is a specific disulfonatostilbene spin label for the Band 3 substrate site (K.F. Schnell, W. Elbe, J. Käsbauer & E. Kaufmann, *Biochim. Biophys. Acta* **732**:266–275, 1983). The pH dependence of NDS-TEMPO binding and of chloride and sulfate binding was studied in resealed human erythrocyte ghosts. pH was varied from 6.0 to 9.0. The ESR spectra from NDS-TEMPO-labeled red cell ghosts exhibited a strong immobilization of membrane-bound NDS-TEMPO. Changes of pH had no effect upon the mobility of membrane-bound NDS-TEMPO. A mutual competition between NDS-TEMPO binding and the binding of the substrate-anions, chloride and sulfate, was observed throughout the entire pH range. The maximal number of NDS-TEMPO binding sites per cell was in the range of 9.0×10^5 to 1.10×10^6 and was found to be insusceptible to changes of pH. The NDS-TEMPO/substrate-site and the chloride/substrate-site dissociation constants amounted to 1.25 μM and to 17 mM and were independent of pH from pH 6.0 to 8.0, while the sulfate/substrate-site dissociation constant displayed a strong pH dependency with a maximum of ~50 mM at about pH 7.0. The NDS-TEMPO inhibition constants from the chloride and the sulfate flux experiments were 0.5 μM (0°C) and 1.8 μM (25°C), respectively, and are in close accordance with the NDS-TEMPO/substrate-site dissociation constants. Our studies provide strong evidence for the assumption that NDS-TEMPO binds in fact to the substrate site of Band 3. They show that the strong pH dependence of the chloride and of the sulfate transport cannot result from the pH dependency of substrate-anion binding, but point to the participation of ionizable regulator sites in transport catalysis. These regulator sites seem to be positioned outside the substrate site of the Band 3 transport domain.

Key Words anion transport · erythrocyte · spin labeling · Band 3

Introduction

The transport of inorganic anions across the erythrocyte membrane is mediated by Band 3, the main intrinsic membrane protein of the red cell membrane. The sulfate (Schnell, 1972; Schnell et al., 1977; Zaki et al., 1975) and the phosphate transport (Deuticke, 1970; Schnell et al., 1981*a*; Berghout et al., 1985) exhibit a pH maximum at about pH 6.4. The chloride fluxes increase from pH 6.0 to 7.0 and show either a flat maximum at approximately pH 7.5 or a plateau depending on the respective experimental conditions (Gunn et al., 1973; Wieth et al., 1973; Dalmark, 1975, 1976; Brahm, 1977; Wieth & Bjerrum, 1982; Wieth et al., 1982). The rate of the sulfate and of phosphate transport are of the same order of magnitude but chloride transport is 3 to 4 orders of magnitude faster than the transport of sulfate or phosphate. On the other hand, a mutual competition between chloride, sulfate and phosphate transport has been observed. (Passow, 1969; Deuticke, 1970; Schnell, 1977; Schnell et al., 1977, 1978; Milanick & Gunn, 1982). These results indicate differences in the transport mechanism in spite of the fact that phosphate, sulfate and chloride are transported by the same transport system. They show that protons are involved in anion transport across the erythrocyte membrane, but they do not provide precise information on their function.

The first information on the role of protons on anion transport comes from the analysis of the flux/concentration curves at different pH. They have shown that the apparent half-saturation constants of chloride (Dalmark, 1975, 1976; Brahm, 1977) and of sulfate (Schnell & Gerhardt, 1973; Schnell et al., 1977; Zaki et al., 1975) increase slightly as pH is elevated and that the phosphate half-saturation constant is completely insusceptible to changes in pH (Schnell et al., 1981). By contrast, the maximal unidirectional fluxes of chloride, sulfate and phosphate exhibit a strong pH dependency. These observations suggest that protons are not essential for substrate anion binding but are required for the translocation of substrate anions across the erythrocyte membrane (Segel, 1975). Jennings (1980), who stud-

ied the chloride/sulfate countertransport in bicarbonate-free solutions, was the first who recognized that sulfate transport across the red cell membrane is associated with a proton cotransport. Milanick and Gunn (1982) have reported an inhibition of the chloride transport by extracellular sulfate which increases as pH is reduced. They observed a random-ordered binding of sulfate and of protons to the erythrocyte membrane. Their results, however, do not provide direct information on whether protons are bound to the substrate site or to a separate site of the Band 3 transport domain.

Anion transport across the red cell membrane appears to be a sequence of complex reactions. Each of these reactions can be modified by protons. For transport, the substrate anions get bound to the Band 3 substrate site which is accessible from the outer and the inner membrane surface. Subsequently, the substrate anion is translocated across the red cell membrane and, finally, it is released at the opposite membrane surface. Anion transport across the red cell membrane appears to be associated with conformational changes of the Band 3 transport domain (Passow, 1982; Knauf et al., 1984; Jennings, 1985). (For review *see* Knauf, 1979; Macara & Cantley, 1983; Passow, 1985). Protons could be involved in substrate anion binding or they could modify the rate of translocation of substrate anions across the erythrocyte membrane.

In order to get direct information on the molecular mechanisms of substrate anion and proton binding, a specific spin probe has to be introduced into the Band 3 substrate site which is capable of indicating conformational or physico-chemical changes of the substrate site. Disulfonatostilbene derivatives have aided substantially to identify Band 3, the anion transport protein, and to elucidate the anion transport mechanism. Disulfonatostilbene compounds like SITS,[1] DIDS, $^3H_2$-DIDS, DNDS and DBDS are nonpenetrating, competitive inhibitors of the anion transport and bind specifically to the Band 3 substrate site (Cabantchik & Rothstein, 1972, 1974; Zaki et al., 1975; Lepke et al., 1976; Ship et al., 1977; Dix et al., 1979; Jennings & Passow, 1979; Rao et al., 1979; Fröhlich, 1982; Furuya et al., 1984). We therefore have synthesized the disulfonatostilbene spin label NDS-TEMPO. The structure of NDS-TEMPO is shown in Fig. 1. Preceding studies have shown that NDS-TEMPO is a nonpenetrating, competitive inhibitor of the chloride and the sulfate transport in human red cell ghosts. Concomitantly, chloride, sulfate and other substrate anions are competitive inhibitors of NDS-TEMPO binding to the erythrocyte membrane (Schnell et al., 1981*c*, 1983). The mutual competition between NDS-TEMPO binding and substrate-anion binding provides strong evidence for the assumption that NDS-TEMPO in fact binds to the substrate site of Band 3. Thus NDS-TEMPO is suited to measure the number of substrate sites per cell and to determine the apparent dissociation constants for substrate anions. At favorable conditions, the membrane-bound fraction of NDS-TEMPO could monitor conformational changes of the Band 3 substrate site in the intact erythrocyte membrane which otherwise are difficult to detect (Schnell et al., 1981*b*).

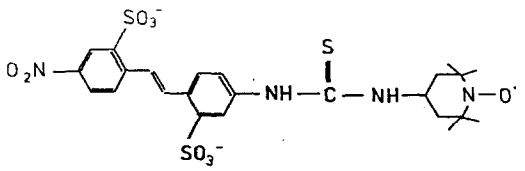

Fig. 1. Structure of NDS-TEMPO. NDS-TEMPO = (N-4-(2,2,6,6-tetramethyl-1-oxyl)piperidinyl-N'-4-(4'-nitro-2,2'-disulfonatostilbene) thiourea, K-salt. Mol wt: 689; purity 96% (HPLC), water soluble. For synthesis and purification *see* Schnell et al. (1983)

This paper is concerned with the pH dependence of NDS-TEMPO, chloride and sulfate binding in relation to chloride and sulfate transport across the erythrocyte membrane. The ESR spectra from NDS-TEMPO-labeled red cell ghosts exhibit a strong immobilization of the membrane-bound fraction of NDS-TEMPO. The mobility of bound NDS-TEMPO was not responsive to changes of pH. Throughout the pH range of 6.0 to 9.0, chloride and sulfate act as competitive inhibitors of NDS-TEMPO binding. The number of substrate sites remains constant from pH 6.0 to 9.0, in contrast to what is to be expected on the basis of the flux measurements. The substrate-site dissociation constants of NDS-TEMPO and of chloride were nearly independent of pH, while the dissociation constants of sulfate display a strong pH responsiveness with a pH maximum at about pH 7.0. In spite of the differences in the binding of chloride and of sulfate to the substrate site, NDS-TEMPO acts as a competitive inhibitor of chloride and of sulfate transport. As studied so far, the inhibition constants of NDS-

[1] ABBREVIATIONS: ANDS, 4-amino-4'-nitro-2,2'-stilbenedisulfonic acid, K salt; BNDS, 4-benzamido-4'-nitro-2,2'-stilbenedisulfonic acid; DADS, 4,4'-diamino-2,2'-stilbenedisulfonic acid, Na salt; DBDS, 4,4'-dibenzoamide-2,2'-stilbenedisulfonic acid, K salt; DIDS, 4,4'-diisothiocyanato-2,2'-stilbenedisulfonic acid, Na salt; DNDS, 4,4'-dinitro-2,2'-stilbenedisulfonic acid, Na salt; FDNB, 1-fluoro-2,4-dinitrobenzene; NCS-TEMPO, 4-isothiocyanato-2,2,6,6-tetramethylpiperidine-1-oxyl; NDS-TEMPO, N-4-(2,2,6,6-tetramethyl-1-oxyl)piperidinyl-N'-4-(4'-nitro-2,2'-stilbenedisulfonic acid) thiourea, K salt; NH_2-TEMPO, 4-amino-2,2,6,6-tetramethylpiperidine-1-oxyl; SITS, 4-acetamido-4'-isothiocyanato-2,2'-stilbenedisulfonic acid.

TEMPO from the flux measurements are consistent with the NDS-TEMPO/substrate-site dissociation constants from the ESR spectroscopy.

Our studies provide strong evidence for the assumption that NDS-TEMPO binds to the substrate site of Band 3. They show that the strong pH dependence of the chloride and of the sulfate transport cannot result from the pH dependency of substrate-anion binding, but point to a participation of ionizable groups outside the substrate site in the regulation of transport catalysis. These "regulator sites," depending upon their ionization, could either facilitate or inhibit the conformational change of the Band 3 transport domain as required for the translocation of the substrate anions across the erythrocyte membrane. In contrast to NDS-TEMPO and chloride binding, a further, ionizable group seems to be involved in sulfate binding to the Band 3 substrate site at low pH.

Materials and Methods

Preparation of the Red Cell Ghosts

Red cell ghosts were prepared by the following procedure (Bodemann & Passow, 1972; Lepke & Passow, 1972; Schnell et al., 1978; Wood & Passow, 1981). Fresh human red cells were washed three times in 10 vol of an isotonic K-citrate solution (20°C, pH 7.3). Plasma and leukocytes were removed. One gram of tightly packed, sedimented red cells (centrifugation 5000 × *g*, 10 min) were added to 1 ml isotonic K-citrate solution to make up a 50% (wt/vol) cell suspension. The suspension was cooled to 0°C. The red cells were then hemolyzed at 0°C, pH 6.2. For this purpose, 10 vol of an ice-cold, hypotonic 2 mM trimagnesiumdicitrate/3.8 mM citric acid solution were added to 1 vol of cell suspension. Five minutes later isotonicity was restored by adding hypertonic K-citrate/KCl or K-citrate/K_2SO_4 solutions (0°C, pH 7.3). The final composition of the resealing solutions was as follows: 0 to 100 mM KCl, or 0 to 100 mM K_2SO_4 and K-citrate, sorbitol, sucrose or Na-gluconate for isosmotic substitution up to 330 mosM. All solutions contained minimally 30 to 40 mM K-citrate which is required for the resealing of the erythrocyte ghosts. The resealing of the red cell ghosts was achieved by incubating them for 45 min at 37°C, pH 7.3. After resealing, the ghosts were titrated to the required pH and washed twice in 20 vol of the resealing solution. The yield of resealed erythrocyte ghosts amounts to approximately 90%. The tonicity of the solutions was checked by means of a microosmometer. The following solutions have a tonicity of 330 mosM and were designated as being isotonic: (in mM) 165 KCl, 132 K_2SO_4, 122 K-citrate, 182 Na-gluconate, 330 sorbitol, 330 sucrose.

ESR Spectra

The ESR spectra were recorded with a Varian E9 ESR spectrometer. 50% suspensions of red cell ghosts were prepared by resuspending ghosts from 1 g red cells in 1 ml of the respective resealing solution. If necessary, the number of ghosts per ml suspensions was counted with a Coulter Counter®. Distinct quantities of NDS-TEMPO were added to the ghost suspensions and the suspensions were carefully mixed. NDS-TEMPO is stable in aqueous solutions. Samples of 70 μl were withdrawn from the suspensions, added into calibrated microhematocrit tubes and placed into the cavity of the ESR spectrometer. The ESR spectra from NDS-TEMPO-labeled red cell ghosts are composite spectra. If necessary, the composite spectra were resolved into a mobile and an immobile component by spectral titration. The addition of 1 mM DNDS causes a complete release of bound NDS-TEMPO from the membrane surface, an increase of the mobile and a disappearance of the immobile signal. Microwave power, modulation amplitude, modulation frequency, scan range, scan time, time constant and receiver gain setting are indicated in the legends of the figures. Because of the high dielectric loss caused by the aqueous solutions, a high microwave power was required for the measurements. Care was taken to avoid distortions of the ESR spectra which could result from saturation effects or inappropriate choice of the scan time and of the time constant (Jost & Griffith, 1976; Schnell et al., 1983). The temperature of the samples was controlled and amounted to 20°C during microwave irradiation.

The concentration of free NDS-TEMPO was determined from the line height of the sharp low-field or the sharp high-field line of the ESR spectra (Jost & Griffith, 1976; Marsh, 1981). Calibration curves of NDS-TEMPO in isotonic (330 mosM) or double-isotonic solutions (660 mosM) of KCl, K_2SO_4, K-citrate, sucrose and sorbitol exhibited a linear relation between line height and NDS-TEMPO concentration over a range of 0.5 to 50 μM. The salt composition of the solution had no effect upon shape and line height of the ESR signal; in double-isotonic solutions the line height of the ESR signal was approximately 2% lower than in isotonic solutions.

The amount of bound NDS-TEMPO was calculated from the concentration of free NDS-TEMPO before and after the addition of 1 mM DNDS to the ghost suspensions. DNDS causes a complete release of bound NDS-TEMPO from the membrane surface without interfering with the ESR spectroscopy. As far as our experiments are concerned, no corrections of the line height of the sharp ESR signal for the underlying broad ESR signal were necessary. The concentration of free NDS-TEMPO was measured after removing the ghosts by centrifugation (50,000 × *g*, 10 min, 20°C) or calculated from the line height of the sharp low-field line and the hematocrit of the ghost suspension.

Flux Measurements

The unidirectional fluxes of chloride and of sulfate were determined under self-exchange conditions (Gardos et al., 1969; Kotyk & Janacek, 1970). The tracer efflux from ^{36}Cl-chloride or ^{35}S-sulfate-labeled, resealed ghosts into a nonradioactive solution was measured. The back-exchange solutions had the same salt composition as the respective resealing solutions and contained additionally 0 to 20 μM NDS-TEMPO. pH of the ghosts and of the back-exchange solutions was titrated to the required values. The tracer efflux measurements were started by adding the radioactively labeled ghosts to the back-exchange solution. The chloride flux experiments were executed with 1% ghost suspensions (1.10×10^8 ghosts/ml suspension) at 0°C by using a filtration technique (Dalmark & Wieth, 1972). The sulfate flux experiments were carried out with 10% ghost suspensions (1.10×10^9 ghosts/ml suspension) at 25°C by means of a centrifugation technique. All fluxes are expressed in mol/(min · g cells), where the term 'g cells' refers to the wet weight of tightly packed red cells. (For details *see* Schnell et al., 1977.)

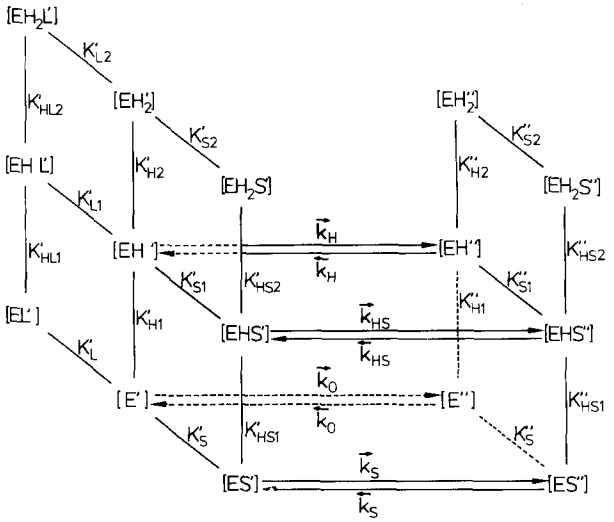

Fig. 2. Diprotonic carrier model for substrate-anion transport across the erythrocyte membrane. *E*, *EH*, *ES*, *EHS*, etc. denote the different states of the carrier. The substrate-anion/carrier dissociation constant, the NDS-TEMPO/carrier dissociation constants and the proton/carrier dissociation constants are designated by K_s, K_L and K_H. k_{HS}, k_s, k_H and k_o are the rate constants for the transport catalysis as mediated by the respective complexes. The arrows on top indicate the direction of the respective reaction as indicated in the figure. The index ' refers to the extracellular surface; the index '' refers to the intracellular surface

Chemicals

NDS-TEMPO was synthesized from ANDS and NH_2-TEMPO according to Schnell et al. (1983). ANDS was a gift from Bayer AG, Leverkusen, FRG. DNDS was purchased from ICN Pharmaceuticals, Plainview, N.Y. NH_2-TEMPO was purchased from EGA-Chemie, Steinheim/Albuch, FRG. Sorbitol was obtained from Serva, Heidelberg, FRG. KCl, K_2SO_4 of G.R. grade, K-citrate, citric acid, pure, trimagnesiumdicitrate and sucrose for biochemical and microbiological use were purchased from Merck, Darmstadt, FRG. $Na^{36}Cl$ and $Na_2{}^{35}SO_4$ were from Amersham-Buchler, Braunschweig, FRG.

Theory

The anion transport domain of Band 3 spans the erythrocyte membrane. The substrate binding site and the transport pathway are composed of hydrophilic and ionizable groups. The transport domain is assumed to function as a carrier where the substrate site is alternately accessible from the outer and the inner membrane surfaces. The pH dependence of the anion transport could result from an activation or an inhibition of substrate-anion binding, from an activation or an inhibition of transport catalysis, or from both of these effects. We assume that the anion transporter carries at least two ionizable groups with an apparent pK in the range of pH 5.0 to 9.0 which participate in anion transport.

A simple diprotic, rapid-equilibrium model for anion transport across the red cell membrane is shown in Fig. 2. The different states of ionization of the anion transporter can be indicated as *E*, *EH* and EH_2, respectively. The index ' refers to the extracellular and the index '' refers to the intracellular surface. The substrate anions are present within the compartment ' and '' while the spin label, NDS-TEMPO, in only present within the extracellular compartment '. We assume that all three forms of the anion carrier are able to bind the substrate anion *S* and the spin label *L*, but only one form of the anion transporter is capable of translocating the bound substrate anion across the red cell membrane. K_s, K_{s1}, K_{s2}, etc., are the dissociation constants for substrate-anion binding at the surfaces ' and '', K_{H1} and K_{H2} are the respective dissociation constants for proton binding and K'_L, K'_{L1} and K'_{L2} are the dissociation constants for NDS-TEMPO binding at the surface '. k_{HS}, k_s, k_H and k_o are the rate constants for the translocation of the respective complexes across the membrane; the arrows indicate the direction of the reaction.

Figure 2 shows that the anion-transport system may exhibit a variety of quite unexpected transport phenomena. In order to reduce the complexity of the transport system we make the following simplifying assumptions:

(1) We assume that *E*, *EH* and EH_2 bind substrate anions *S* and NDS-TEMPO *L* equally well and that substrate-anion binding and NDS-TEMPO binding have no effect upon the binding of protons. From these assumptions it follows that:

$$K'_s = K'_{s1} = K'_{s2} \qquad K''_s = K''_{s1} = K''_{s2}$$
$$K'_{H1} = K'_{HS1} = K'_{HL1} \qquad K''_{H1} = K''_{HS1} = K''_{HL1}$$
$$K'_{H2} = K'_{HS2} = K'_{HL2} \qquad K''_{H2} = K''_{HS2}.$$

(2) Furthermore, we assume for convenience that K'_{H1} and K''_{H1} are equal to K'_{H2} and K''_{H2}.

(3) We assume that the proton transport across the red cell membrane can be neglected at our experimental conditions. Therefore the rate constants $\vec{k}_H$ and $\overleftarrow{k}_H$ were set to zero.

(4) Finally, we assume the chloride transport to be mediated by *ES* while the sulfate transport is catalyzed by *EHS*. Thus for chloride transport, the rate constants $\vec{k}_{HS}$ and $\overleftarrow{k}_{HS}$ were set to zero while, for sulfate transport, the rate constants $\vec{k}_s$ and $\overleftarrow{k}_s$ were set to zero.

For the derivation of the NDS-TEMPO binding equation and of the anion transport equations, we start with the equation of conservation of matter which states that the total carrier concentration E_T is equal to the sum of the different states of the carrier at both membrane sides:

$$E_T = E' + EH' + EH_2' + ES' + EHS' + EH_2S' + EL' + EHL' + EH_2L' + E'' + EH'' + EH_2'' + ES'' + EHS'' + EH_2S''. \quad (1)$$

In addition, we get a set of mass law equations for the reactions taking place at the surfaces ′ and ″:

$$E' \cdot H' = K_{H1} \cdot EH' \quad (2)$$
$$E'' \cdot H'' = K_{H1} \cdot EH'' \quad (3)$$
$$EH' \cdot H' = K_{H2} \cdot EH_2' \quad (4)$$
$$EH'' \cdot H'' = K_{H2} \cdot EH_2'' \quad (5)$$
$$E' \cdot S' = K_s' \cdot ES' \quad (6)$$
$$E'' \cdot S'' = K_s'' \cdot ES'' \quad (7)$$
$$EH' \cdot S' = K_s' \cdot EHS' \quad (8)$$
$$EH'' \cdot S'' = K_s'' \cdot EHS'' \quad (9)$$
$$EH_2' \cdot S' = K_s' \cdot EH_2S' \quad (10)$$
$$EH_2'' \cdot S'' = K_s'' \cdot EH_2S'' \quad (11)$$
$$E' \cdot L' = K_L' \cdot EL' \quad (12)$$
$$EH' \cdot L' = K_L' \cdot EHL' \quad (13)$$
$$EH_2' \cdot L' = K_L' \cdot EH_2L'. \quad (14)$$

The steady-state equations for the empty carrier, for chloride and for sulfate transport read:

$$\vec{k}_o \cdot E' = \overleftarrow{k}_o \cdot E'' \quad (15)$$
$$\vec{k}_s \cdot ES' + \vec{k}_o \cdot E' = \overleftarrow{k}_s \cdot ES'' + \overleftarrow{k}_o \cdot E'' \quad (16)$$
$$\vec{k}_{HS} \cdot EHS' + \vec{k}_o \cdot E' = \overleftarrow{k}_{HS} \cdot EHS'' + \overleftarrow{k}_o \cdot E''. \quad (17)$$

L_B, the total concentration of bound NDS-TEMPO, is given by:

$$L_B = EL' + EHL' + EH_2L'. \quad (18)$$

The unidirectional chloride and sulfate fluxes are assumed to be proportional to the concentration of the substrate-anion/carrier complex at the *cis*-surface of the membrane and can be written as:

$$\vec{J}_{Cl} = \vec{k}_s \cdot ES' \quad (19)$$
$$\overleftarrow{J}_{Cl} = \overleftarrow{k}_s \cdot ES'' \quad (20)$$
$$\vec{J}_S = \vec{k}_{HS} \cdot EHS' \quad (21)$$
$$\overleftarrow{J}_S = \overleftarrow{k}_{HS} \cdot EHS''. \quad (22)$$

$\vec{J}_{Cl}$ and $\vec{J}_S$ are the unidirectional fluxes of chloride and of sulfate from compartment ′ to ″ while $\overleftarrow{J}_{Cl}$ and $\overleftarrow{J}_S$ are the unidirectional fluxes of chloride and of sulfate from compartment ″ to ′, respectively. k_s, k_{HS} and ES, EHS denote the rate constants for the translocation and the respective substrate-anion/carrier complexes as indicated in Fig. 2.

Substituting the mass law Eqs. (2)–(14) into the equation of conservation of matter (Eq. 1) and eliminating all forms of E'' by means of the steady-state Eqs. (15)–(17), E', ES' and EHS' can be expressed as functions of S', S'', H', H'', the substrate anion and the proton concentrations in the compartment ′ and ″. Upon resubstitution of E', ES' and EHS' into the Eqs. (18), (19) and (21), the NDS-TEMPO binding equation and the unidirectional flux equations for chloride and sulfate read as indicated by Eqs. (23)–(25):

$$L_B = \frac{E_T L'}{K_L'((1 + S'/K_s') + (\vec{k}_o/\overleftarrow{k}_o)(1 + S''/K_s'')) + L'}; \quad (23)$$

$$\vec{J}_{Cl} = \frac{\vec{k}_s(\overleftarrow{k}_o K_s'' + \overleftarrow{k}_s S'')E_T S'}{(\overleftarrow{k}_o K_s'' + \overleftarrow{k}_s S'')A'(K_s'(1 + L'/K_L') + S') + (\vec{k}_o K_s' + \vec{k}_s S')A''(K_s'' + S'')} \quad (24)$$

with

$$A' = 1 + (H'/K_{H1})(1 + H'/K_{H2}) \qquad A'' = 1 + (H''/K_{H1})(1 + H''/K_{H2});$$

$$\vec{J}_S = \frac{\vec{k}_{HS}(\overleftarrow{k}_o K_s'' + \overleftarrow{k}_{HS} S'')E_T S'}{(\overleftarrow{k}_o K_s'' + \overleftarrow{k}_{HS} S'')B'(K_s'(1 + L'/K_L') + S') + (\vec{k}_o K_s' + \vec{k}_{HS} S')B''(K_s'' + S'')} \quad (25)$$

with

$$B' = 1 + K_{H1}/H' + H'/K_{H2} \qquad B'' = 1 + K_{H1}/H'' + H''/K_{H2}.$$

Table 1. Equations for NDS-TEMPO binding and substrate-anion transport by a diprotic carrier transport model[a]

NDS-TEMPO Binding: $S' = S''$; $H' = H''$; $K'_{H1} = K''_{H1}$; $K'_{H2} = K''_{H2}$

$$L_{B(\max)} = E_T \quad (28) \qquad K_{L(\text{app}/S)} = K'_L\left(1 + a + \frac{aK'_s + K''_s}{K'_sK''_s}S\right) \quad (29)$$

Flux Measurements: $S' = S''$; $H' = H''$; $K'_{H1} = K''_{H1}$; $K'_{H2} = K''_{H2}$

$$\vec{J}_{\max(\text{Cl})} = \frac{\vec{k}_s\tilde{k}_sE_T}{A(\vec{k}_s + \tilde{k}_s)} \quad (30) \qquad \vec{J}_{\max(S)} = \frac{\vec{k}_{HS}\tilde{k}_{HS}E_T}{B(\vec{k}_{HS} + \tilde{k}_{HS})} \quad (31)$$

$$K_{m(\text{app}/L)} = \frac{K'_sK''_s(1 + a + L'/K'_L)}{aK'_s + K''_s} \quad (32) \qquad K_{iL(\text{app}/S)} = K'_L\left(1 + a + \frac{aK'_s + K''_s}{K'_sK''_s}S\right) \quad (33)$$

Detailed Balance: $K'_{H1} = K''_{H1}$

Chloride: $\vec{k}_s\tilde{k}_oK''_s = \vec{k}_s\tilde{k}_oK'_s$ (34) Sulfate: $\vec{k}_{HS}\tilde{k}_oK''_s = \vec{k}_{HS}\tilde{k}_oK'_s$ (35)

Definitions: $a = \vec{k}_o/\tilde{k}_o$ $A = 1 + (H/K_{H1})(1 + H/K_{H2})$ $B = 1 + K_{H1}/H + H/K_{H2}$

[a] L_B, L are the concentrations of bound and of free NDS-TEMPO, $L_{B(\max)}$ is the maximum NDS-TEMPO binding capacity and E_T the total carrier concentration. $K_{L(\text{app}/S)}$ is the apparent NDS-TEMPO/carrier dissociation constant at a fixed S, S is the substrate-anion concentration and H the proton concentration. $\vec{J}_{\max}$, $K_{m(\text{app}/L)}$ and $K_{iL(\text{app}/S)}$ are the maximal unidirectional flux of chloride (subscript Cl) and of sulfate (subscript S), the apparent half-saturation constant of chloride and sulfate at a fixed NDS-TEMPO concentration and the apparent NDS-TEMPO inhibition constant from the L-axis intercept of the Dixon plots at a constant substrate-anion concentration. K_s and K_L are the anion/substrate-site dissociation constant and the NDS-TEMPO/substrate-site dissociation constant, K_{H1} and K_{H2} are the proton dissociation constants of the first and the second prototropic, transport regulator site. The indices ' and " refer to the extracellular and the intracellular membrane surface. $\vec{k}_{HS}$, $\tilde{k}_{HS}$, $\vec{k}_s$, $\tilde{k}_s$, $\tilde{k}_o$ and $\vec{k}_o$ are the rate constants of the translocation. (For definition *see* Fig. 2.)

The inspection of Eqs. (23)–(25) shows that, for the above conditions, NDS-TEMPO binding is independent of pH while the unidirectional fluxes of chloride and of sulfate exhibit a clear pH dependency. The effects of pH on NDS-TEMPO binding and on anion transport are summarized in Table 1: The maximal unidirectional fluxes of chloride and of sulfate exhibit a pH dependency, while the maximum NDS-TEMPO binding capacity, the NDS-TEMPO/substrate-site dissociation constant, the apparent half-saturation constant for the self-exchange fluxes, and the NDS-TEMPO inhibition constant are independent of pH. The principle of detailed balance imposes some restraints upon the system and not all of the rate constants and the dissociation constants can be chosen deliberately. The restraints are given by Eqs. (34) and (35) (Table 1). (For details *see* Heinz, 1978 and Segel, 1975.)

Plotting Procedures

At self-exchange conditions, the substrate-anion concentrations and pH at both membrane sides are equal and the indices of S and of H in Eqs. (23)–(25) can be dropped. The oppositely directed unidirectional fluxes of the substrate anion from compartment ' to " and from compartment " to ' are equal in magnitude and we need consider only one of them. For plotting procedures, the NDS-TEMPO binding equation (Eq. 23) can be rearranged to give a Michaelis-Menten type of equation:

$$L_B = L_{B(\max)}\frac{L_f}{K_{L(\text{app}/S)} + L_f}. \quad (26)$$

Correspondingly, the flux equations for the unidirectional chloride (Eq. 24) and the unidirectional sulfate flux (Eq. 25) can be written as:

$$\vec{J} = \vec{J}_{\max}\frac{S}{K_{m(\text{app}/L)} + S}. \quad (27)$$

For definitions of the symbols *see below*. The definition of $L_{B(\max)}$, $K_{L(\text{app}/S)}$, $\vec{J}_{\max}$ and $K_{m(\text{app}/L)}$ in terms of the carrier transport model are given in Table 1.

In order to maintain isotonicity, isosmotic substitution was made by an impermeable nonelectrolyte such as sucrose or sorbitol or by a nonpenetrating salt like K-citrate. All solutions contain 40 mM K-citrate which is inevitable for a proper resealing of the erythrocyte ghosts. There is some evidence that citrate^{2-} acts as a competitive inhibitor of NDS-TEMPO binding and of anion transport whereas citrate^{3-} appears to be ineffective. For nonelectrolyte substitution, the total citrate concentration is constant and the concentration of divalent citrate is given by:

$$I_2 = I_T(1 + K_3/H). \quad (36)$$

Thus the equation for NDS-TEMPO binding and the flux equation can be rewritten as:

$$L_B = L_{B(\max)} \frac{L_f}{K_L(1 + S/K_s + I_2/K_{i2}) + L_f} \quad (37)$$

$$\vec{J} = \vec{J}_{\max} \frac{S}{K_s(1 + L_f/K_L + I_2/K_{i2}) + S}. \quad (38)$$

For K-citrate substitution, on the other hand, the total citrate concentration is a function of the substrate-anion concentration S, and I_2 is given by:

$$I_2 = (1 - S/S_o)I_{o2} \quad (39)$$

with

$$I_{o2} = I_o/(1 + K_3/H). \quad (40)$$

Substituting Eqs. (39) and (40) into Eqs. (37) and (38), the NDS-TEMPO binding equation and the flux equation read:

$$L_B = L_{B(\max)} \frac{L_f}{K_L(1 + I_{o2}/K_{i2} + (1 - I_{o2}K_s/(S_oK_{i2}))S/K_s) + L_f} \quad (41)$$

$$\vec{J} = \vec{J}_{\max} \frac{S}{K_s(1 + L_f/K_L + I_{o2}/K_{i2}) + (1 - I_{o2}K_s/(S_oK_{i2}))S}. \quad (42)$$

L_B, $L_{B(\max)}$ and L_f denote the bound NDS-TEMPO, the maximal binding capacity for NDS-TEMPO and the concentration of free NDS-TEMPO. $\vec{J}$ and $\vec{J}_{\max}$ are the unidirectional flux of the substrate anion S and the maximal unidirectional flux of S. S is the substrate-anion concentration, H the proton concentration, I_2 and I_{o2} are the concentrations of divalent citrate at nonelectrolyte substitution and at K-citrate substitution. K_L, K_s and K_{i2} are the substrate-site dissociation constants of NDS-TEMPO, substrate anions and citrate^{2-} of Band 3. I_T, I_o and S_o indicate the total citrate concentration at nonelectrolyte substitution, the citrate and the substrate-anion concentration of isotonic K-citrate and of isotonic substrate-anion solutions. K_3 is the dissociation constant of the third dissociation step of citric acid which amounts to 6.4×10^{-7} M at 20°C (Weast & Melvin, 1982–1983).

The apparent NDS-TEMPO/substrate-site dissociation constant, the apparent NDS-TEMPO inhibition constants, the apparent half-saturation constants from the plots for nonelectrolyte or K-citrate substitution and the equations for the replots are compiled in Table 2. K_L, K_s and K_{i2} are complex magnitudes; the definitions are given in Table 2. I_T and I_o are constants, but I_2 and I_{o2} are functions of pH (Table 2, Eqs. 36, 39–42).

NDS-TEMPO Binding

The data of NDS-TEMPO binding studies were analyzed by double-reciprocal plots of $1/L_B$ versus $1/L_f$ (Klotz plot) and by the plots of L_f/L_B versus L_f (Hanes-Woolf plot). $L_{B(\max)}$ and $K_{L(\text{app}/S)}$ were obtained, as usual, from the intercepts and the slopes of the plots. L_B, L_f and $L_{B(\max)}$ denote the bound NDS-TEMPO, the free NDS-TEMPO and the maximum binding capacity of the suspension, $K_{L(\text{app}/S)}$ is the apparent NDS-TEMPO/substrate-site dissociation constant at a fixed concentration of S. Both the Klotz plot and the Hanes-Woolf plot were always linear and exhibited a competitive inhibition of NDS-TEMPO binding by chloride and by sulfate irrespective of whether isosmotic substitution had been made by sorbitol, sucrose or K-citrate (Eqs. 37 and 41). The plots give the true $L_{B(\max)}$, but $K_{L(\text{app}/S)}$ as obtained from the plots is a function of the substrate anion concentration S and the citrate^{2-} concentration I_2 or I_{o2} (Table 2, Eqs. 43 and 44). The replots of $K_{L(\text{app}/S)}$ versus S give $K_{L(\text{app})}$, the apparent NDS-TEMPO dissociation constant at zero substrate-anion concentration, and $K_{s(\text{app})}$, the apparent substrate-anion dissociation constant at zero NDS-TEMPO concentration (Table 2, Eqs. 43.1–44.2). The replots of $K_{L(\text{app})}$ and $K_{s(\text{app})}$ versus I_2 or I_{o2} (Table 2, Eqs. 43.1–44.1) and the replots of $K_{s(\text{app})}$ versus $(1 + K_{s(\text{app})}/S_o)I_{o2}$ (Table 2, Eq. 49) provide K_L, K_s and K_{i2}, respectively.

Flux Measurements

The unidirectional fluxes of chloride and of sulfate were measured at self-exchange conditions by means of ^{36}Cl-chloride and ^{35}S-sulfate. The flux/concentration curves were analyzed by means of the Lineweaver-Burk plot or by means of the Hanes-Woolf plot. Isosmotic substitution was made with either sorbitol or sucrose. The plots give $\vec{J}_{\max}$, the true maximal unidirectional flux and $K_{m(\text{app}/L)}$, the apparent half-saturation constant of the substrate-anion S at a fixed concentration of NDS-TEMPO (Table 2, Eqs. 45 and 46). $K_{m(\text{app}/L)}$ can be further analyzed by appropriate replots (Table 2, Eqs. 45.1–46.2).

The inhibition of chloride and of sulfate transport by NDS-TEMPO was studied by means of the Dixon plot. Isosmotic substitution was made by K-citrate or by an impermeable nonelectrolyte. For nonelectrolyte substitution, 40 mM K-citrate, the family of Dixon plots always intersects above the abscissa, but the intersection of the straight lines may give too high a value for the NDS-TEMPO inhibition constant. For K-citrate substitution, the Dixon plots may intersect above, on or below the

Table 2. Equations for replotting[a]

Nonelectrolyte substitution		K-citrate substitution	
$K_{L(app/S)} = K_L(1 + I_2/K_{i2} + S/K_s)$	(43)	$K_{L(app/S)} = K_L(1 + (1 - S/S_o)I_{o2}/K_{i2} + S/K_s)$	(44)
$K_{L(app)} = K_L(1 + I_2/K_{i2})$	(43.1)	$K_{L(app)} = K_L(1 + I_{o2}/K_{i2})$	(44.1)
$K_{s(app)} = K_s(1 + I_2/K_{i2})$	(43.2)	$K_{s(app)} = \frac{K_s(1 + I_{o2}/K_{i2})}{1 - K_s I_{o2}/(K_{i2}S_o)}$	(44.2)
$K_{m(app/L)} = K_s(1 + I_2/K_{i2} + L_f/K_L)$	(45)	$K_{m(app/L)} = \frac{K_s(1 + I_{o2}/K_{i2} + L_f/K_L)}{1 - I_{o2}K_s/(S_o K_{i2})}$	(46)
$K_{m(app)} = K_s(1 + I_2/K_{i2})$	(45.1)	$K_{m(app)} = K_s(1 + I_{o2}/K_{i2})/(1 - K_s I_{o2}/(K_{i2}S_o))$	(46.1)
$K_{iL(app)} = K_L(1 + I_2/K_{i2})$	(45.2)	$K_{iL(app)} = K_L(1 + I_{o2}/K_{i2})$	(46.2)
$K_{iL(app/S)} = K_L(1 + I_2/K_{i2} + S/K_L)$	(47)	$K_{iL(app/S)} = K_s(1 + (1 - S/S_o)I_{o2}/K_{i2} + S/K_s)$	(48)
$K_{iL(app)} = K_L(1 + I_2/K_{i2})$	(47.1)	$K_{iL(app)} = K_L(1 + I_{o2}/K_{i2})$	(48.1)
$K_{m(app)} = K_L(1 + I_2/K_{i2})$	(47.2)	$K_{m(app)} = \frac{K_s(1 + I_{o2}/K_{i2})}{1 - K_s I_{o2}/(K_{i2}S_o)}$	(48.2)
$K_{s(app)} = K_s(1 + (1 + K_{s(app)}/S_o)I_{o2}/K_{i2})$	(49)	$K_{m(app)} = K_s(1 + (1 + K_{m(app)}/S_o)I_{o2}/K_{i2})$	(50)

Definitions:

$$a \equiv \vec{k}_o/\bar{k}_o \qquad K_L \equiv (1 + a)K'_L \qquad K_s \equiv \frac{(1 + a)K'_s K''_s}{aK'_s + K''_s} \qquad K_{i2} \equiv \frac{(1 + a)K'_{i2}K''_{i2}}{aK'_{i2} + K''_{i2}}$$

[a] $K_{L(app/S)}$, $K_{iL(app/S)}$ and $K_{m(app/L)}$ are the NDS-TEMPO/substrate-site dissociation constant at constant S, the NDS-TEMPO inhibition constant from the L_f-axis intercept of the Dixon plot at constant S and the apparent half-saturation constant of the substrate anion S at a fixed concentration of NDS-TEMPO. $K_{L(app)}$, $K_{s(app)}$, $K_{m(app)}$ and $K_{iL(app)}$ are the respective constants at zero substrate-anion and zero NDS-TEMPO concentration. K_L, K_s and K_{i2} are the NDS-TEMPO/substrate-site, the substrate-anion/substrate site and the citrate^{2-}/substrate-site dissociation constants. The definitions indicate the meaning of a, K_L, K_s and K_{i2} in terms of the diprotic rapid-equilibrium anion transport model shown in Fig. 2. S and S_o are the substrate-anion concentration and the substrate-anion concentration of an isotonic solution, L_f is the concentration of free NDS-TEMPO, I_2 and I_{o2} are the concentrations of divalent citrate for nonelectrolyte substitution and for K-citrate substitution, respectively. $\vec{k}_o$ and $\bar{k}_o$ are the rate constants for the translocation of the empty carrier from compartment ′ to ″ and in the reverse direction, K'_s, K''_s, K'_{i2}, K''_{i2} and K'_L are the true dissociation constants of the substrate anion, citrate^{2-} and NDS-TEMPO at the surfaces ′ and ″, respectively. (*Compare* Fig. 2.)

abscissa, depending on the relative affinities of the substrate and the substitute anion, and the Dixon plots could indicate a noncompetitive or a mixed-type inhibition instead of a competitive inhibition.

For a pure, competitive inhibition, the intersection point of the Dixon plots at two different fixed substrate-anion concentrations provides the NDS-TEMPO inhibition constant and the maximal flux of the substrate anion. However, for a more precise evaluation of the data, the intercepts on the L_f axis together with appropriate replots have been employed. The L_f-axis intercepts for nonelectrolyte substitution and for K-citrate substitution provide $K_{iL(app/S)}$, the apparent inhibition constant of NDS-TEMPO at the substrate-anion concentration S (Table 2, Eqs. 47 and 48). The replots of $K_{iL(app/S)}$ versus S furnish $K_{iL(app)}$ and $K_{m(app)}$, the NDS-TEMPO inhibition constant at zero substrate-anion concentration and the half-saturation constant at zero NDS-TEMPO concentration (Table 2, Eqs. 47.1–48.2). In order to eliminate the effects of citrate^{2-} on NDS-TEMPO and substrate-anion binding, $K_{iL(app)}$ and $K_{m(app)}$ have to be replotted versus I_2, I_{o2} or $(1 + K_{m(app)}/S_o)I_{o2}$. These replots yield K_L, K_s and K_{i2} (Table 2, Eqs. 47.1–48.1 and 50).

Replots

$K_{L(app/S)}$, the apparent NDS-TEMPO/substrate-site dissociation constant, and $K_{iL(app/S)}$, the apparent NDS-TEMPO inhibition constant at a fixed concentration of the substrate-anion S, are complex magnitudes which can be further analyzed by appropriate replots (Table 2, Eqs. 47 and 48). The replots of $K_{L(app/S)}$ versus S and the replots of $K_{iL(app/S)}$ versus S should be linear. The intercepts on the $K_{L(app/S)}$ or the $K_{iL(app/S)}$ axis give $K_{L(app)}$, the NDS-TEMPO/

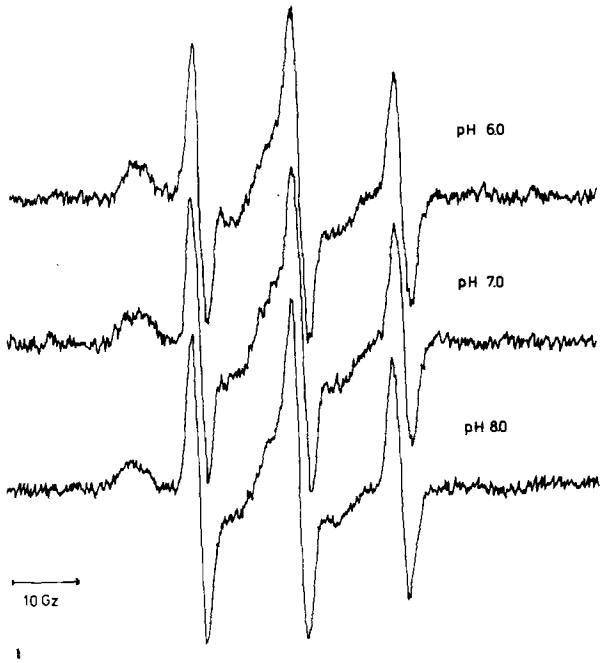

Fig. 3. ESR spectra from suspensions of NDS-TEMPO-labeled human erythrocyte ghosts at different pH. The ESR spectra are constituted of an immobile and of a mobile component corresponding to membrane-bound and to free NDS-TEMPO. 10 μM NDS-TEMPO, 80% suspension of erythrocyte ghosts in 122 mM K-citrate solution (330 mosM), 25°C, pH as indicated in the figure. Field strength: 0.34 T, microwave: 100 kHz, modulation amplitude: 0.5 mT, microwave power: 50 mW, receiver gain setting: 8×10^3, scan time/filter time constant: 16 min/3 sec. 10 Gz = 1 mT

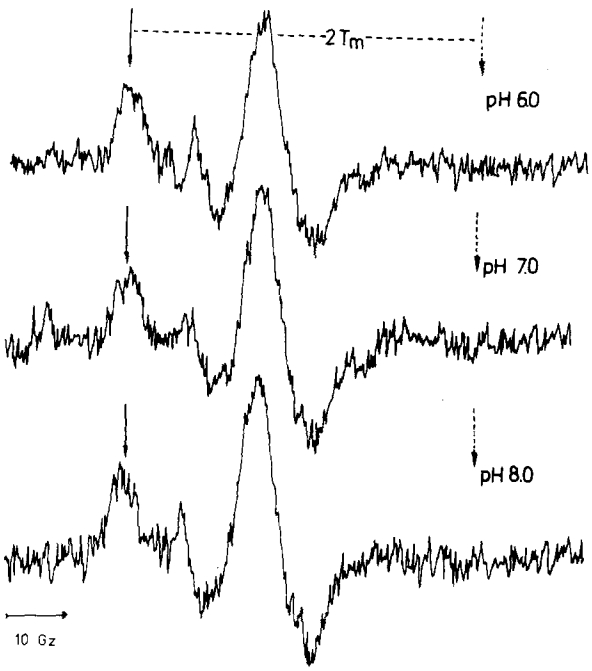

Fig. 4. pH dependence of the immobile component of the ESR spectra. Same ESR spectra as shown in Fig. 3 upon subtraction of the mobile signal by the spectral titration technique (Jost & Griffith, 1976). 10 Gz = 1 mT

substrate-site dissociation constant, and $K_{iL(app)}$ the NDS-TEMPO inhibition constant at zero substrate-anion concentration. The S-axis intercepts provide $K_{S(app)}$ and $K_{m(app)}$, the apparent dissociation constant of substrate anion/substrate site and the apparent half-saturation constant of the substrate anion at zero NDS-TEMPO concentration. $K_{L(app)}$, $K_{iL(app)}$, $K_{s(app)}$ and $K_{m(app)}$ for nonelectrolyte and for K-citrate substitution are listed in Table 2. The definitions of the symbols are given in the legend to the table.

Results

Figure 3 shows ESR spectra from NDS-TEMPO-labeled red cell ghosts at different pH. The ghosts were resealed and resuspended in isotonic 122 mM K-citrate solutions. 80% suspensions of ghosts were used to which 10 μM NDS-TEMPO were added. The ESR spectra from the suspensions of red cell ghosts are composite spectra which consist of a sharp three-line signal and a broad, comparatively weak, immobile signal.

The immobile signal arises from the fraction of membrane-bound NDS-TEMPO and provides information on the mobility of bound NDS-TEMPO. By spectral titration, the composite ESR spectra were resolved into a mobile and an immobile component. The immobile component of the ESR spectra is shown in Fig. 4. The outer hyperfine splitting, 2 T_m, as far as it could be assessed, amounts to approximately 6.3 mT and is not affected by pH. In addition, the distance between the broad low-field line and the central line remains constant. These findings indicate that changes of pH have no effect upon the mobility of membrane-bound NDS-TEMPO.

The effect of chloride and sulfate on NDS-TEMPO binding is shown in Fig. 5. The experiments were performed with 50% suspensions of resealed red-cell ghosts at self-exchange conditions. K-citrate was used for isotonic substitution. The double-reciprocal plots of bound versus free NDS-TEMPO are linear and intersect on the ordinate. The Klotz plots increase in slope as the substrate-anion concentration is elevated (Fig. 5). Correspondingly, the Hanes-Woolf plots of L_f/L_B versus

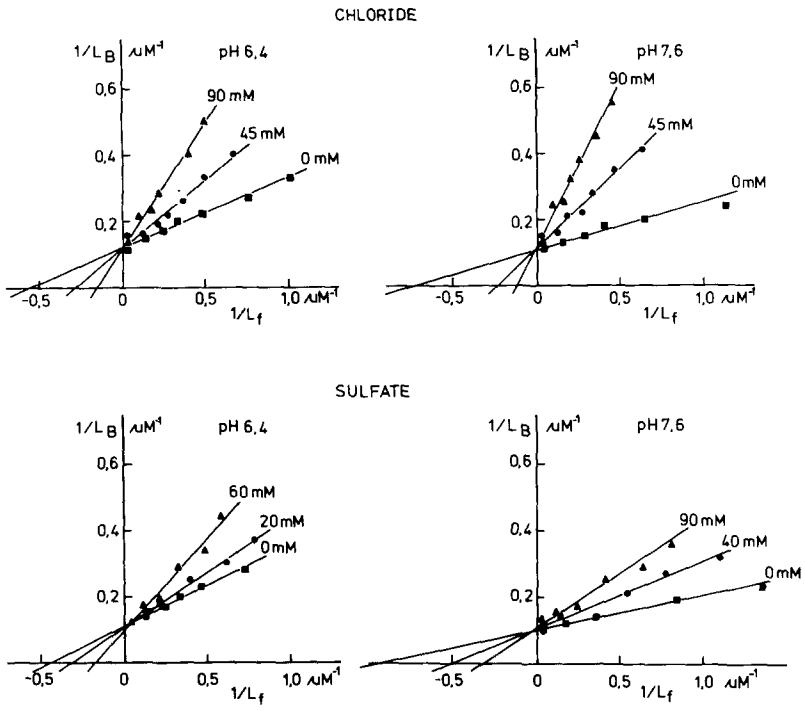

Fig. 5. Effects of chloride and of sulfate on NDS-TEMPO binding in human erythrocyte ghosts at different pH. Ordinate: $1/L_B$ (μmol/liter suspension)$^{-1}$, abscissa: $1/L_f$ (μM)$^{-1}$; L_B and L_f are the concentrations of bound and of free NDS-TEMPO. 50% suspension of resealed red cell ghosts, pH, chloride and sulfate concentrations as indicated in the figure. Isosmotic substitution to 330 mosM by K-citrate

Table 3. pH Dependence of NDS-TEMPO, chloride and sulfate binding to resealed human erythrocyte ghosts[a]

pH	$L_{B(max)}$ (nmol/g cells)	$K_{L(app)}$ (μM)	$K_{s(app/Cl)}$ (mM)	$K_{s(app/SO_4)}$ (mM)
6.0	16.25 ± 1.95	2.97 ± 0.73	42 ± 10	18 ± 5
6.4	18.25 ± 1.30	2.35 ± 0.57	32 ± 8	34 ± 8
6.8	19.19 ± 1.12	1.90 ± 0.34	27 ± 5	75 ± 12
7.2	18.44 ± 1.02	1.55 ± 0.26	21 ± 3	72 ± 9
7.6	20.02 ± 1.30	1.28 ± 0.14	21 ± 3	40 ± 7
8.0	20.40 ± 1.30	1.28 ± 0.10	19 ± 4	30 ± 5
9.0	19.96 ± 1.49	2.13 ± 0.28	24 ± 7	—

[a] $L_{B(max)}$ is the maximal NDS-TEMPO binding capacity/g cells wet weight, $K_{L(app)}$ the apparent NDS-TEMPO dissociation constant at zero substrate anion concentration, and $K_{s(app/Cl)}$ and $K_{s(app/SO_4)}$ are the apparent dissociation constants of chloride and of sulfate at zero NDS-TEMPO concentration as obtained from the Klotz plot or the Hanes-Woolf plot. All experiments were conducted with 50% suspensions of resealed red cell ghosts (5.5×10^9 ghosts/ml suspension) at 20°C. Isosmotic substitution by K-citrate, pH as indicated in the table.

L_f were linear too and exhibited a parallel shift as the substrate-anion concentration was raised (*not shown*). These features are indicative of a competitive inhibition. $L_{B(max)}$, the maximum binding capacity of NDS-TEMPO and $K_{L(app/S)}$, the apparent NDS-TEMPO/substrate-site dissociation constant were obtained as usual from the slope and the intercepts of the plots. The Klotz plot and the Hanes-Woolf plot give the true $L_{B(max)}$ irrespective of whether isosmotic substitution has been made by a nonelectrolyte or by K-citrate (Eqs. 26, 37 and 41). The replots of $K_{L(app/S)}$ versus the chloride or the sulfate concentration were linear and provide $K_{L(app)}$, the apparent NDS-TEMPO/substrate-site dissociation constant at zero substrate-anion concentration, $K_{S(app/Cl)}$ and $K_{S(app/SO_4)}$, the apparent chloride/substrate-site and sulfate/substrate-site dissociation constants at zero NDS-TEMPO concentration (Table 2, Eqs. 43–44.2).

The results of the NDS-TEMPO equilibrium binding studies are listed in Table 3. The maximum NDS-TEMPO binding capacity is in the range of 16.2 to 20.5 nmol/g cells corresponding to 9.0×10^5 to 1.10×10^6 NDS-TEMPO binding sites per cell.

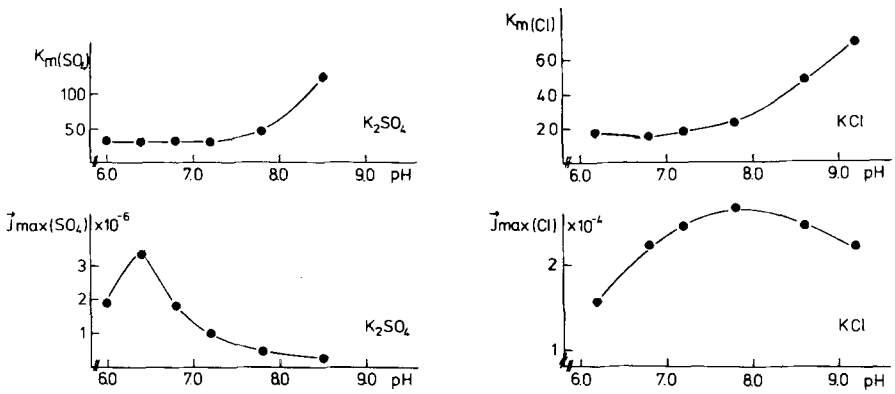

Fig. 6. pH dependence of the maximal unidirectional fluxes and of the half-saturation constants of chloride and of sulfate. $\vec{J}_{max(Cl)}$ and $\vec{J}_{max(SO_4)}$ mol/(min · g cells) are the maximum chloride and the maximum sulfate flux, $K_{m(Cl)}$ and $K_{m(SO_4)}$ are the apparent half-saturation constants from the flux/concentration curves. Chloride concentrations from 5 to 100 mM and sulfate concentrations from 10 to 100 mM were used. The chloride flux experiments were carried out with 1% suspensions of resealed erythrocyte ghosts at 0°C, isoosmotic substitution was made by sorbitol. The sulfate flux measurements were performed with 10% suspensions of red cell ghosts at 25°C, isosmotic substitution by sucrose. All solutions contain 40 mM K-citrate. No corrections for citrate^{2-} inhibition have been made

The maximal NDS-TEMPO binding capacity is independent of pH; the slight decrease at pH 6.0 is statistically not significant. The apparent NDS-TEMPO/substrate-site dissociation constants decrease from approximately 3.0 μM at pH 6.0 to 1.3 μM at pH 7.6. Above pH 8.0, an increase of the pH results in a slight increase of the NDS-TEMPO dissociation constant. The apparent chloride/substrate-site dissociation constants exhibit a similar pattern of pH responsiveness. By contrast, the sulfate/substrate-site dissociation constants show a different pH profile with a pH maximum at about pH 7.0.

Figure 6 shows the pH dependence of the maximal unidirectional fluxes of chloride and of sulfate and the apparent half-saturation constants for the chloride and the sulfate self-exchange. The chloride flux experiments were performed at 0°C; isosmotic substitution was made by sorbitol. The sulfate flux measurements were conducted at 25°C; isosmotic substitution was made by sucrose. The chloride and the sulfate concentrations ranged from 5 to 100 mM. The flux/concentration curves at a fixed pH were analyzed by the Lineweaver-Burk plot and the Hanes-Woolf plot which gave identical results. For our experimental conditions, the maximal unidirectional chloride flux exhibits a maximum at about pH 7.8 while the maximal unidirectional sulfate flux has a maximum at approximately pH 6.4. From pH 6.0 to 8.0, the chloride and the sulfate half-saturation constants were only slightly modified by pH. Above pH 8.0, the half-saturation constants for the chloride and the sulfate self-exchange increase.

NDS-TEMPO acts as a competitive inhibitor of the chloride and the sulfate transport in resealed erythrocyte ghosts (Fig. 7). For technical reasons the chloride flux measurements were executed at 0°C, while the sulfate flux measurements were performed at 25°C. Again K-citrate has been employed for isosmotic substitution. The Dixon plots display a competitive type of inhibition. For a pure, competitive inhibition, the intersection of the straight lines provides the inhibition constant, but for our experimental conditions, the intersection point gives $K_{iL(app)} = K_L(1 + I_{o2}/K_{i2})$. In order to improve the accuracy of the plotting procedure, $K_{iL(app/S)}$, the NDS-TEMPO inhibition constant at a fixed concentration of S was read from the L_f-axis intercept. The $K_{iL(app/S)}$ versus S replots from a series of experiments give $K_{iL(app)}$ and $K_{m(app)}$ (Table 2, Eqs. 48–48.2).

The NDS-TEMPO inhibition constant at zero substrate anion concentration and the apparent half-saturation constants of chloride and of sulfate at zero NDS-TEMPO concentration are summarized in Table 4. The inhibition constant of NDS-TEMPO and the half-saturation constants of chloride and sulfate decrease with increasing pH. Upon correction for the citrate^{2-} inhibition, the inhibition constant of NDS-TEMPO and the half-saturation constants of chloride and sulfate were independent of pH. The NDS-TEMPO inhibition constant from the chloride and the sulfate flux measurements were 0.5 and 1.8 μM. The slight differences arise probably from the different temperatures which were used for the chloride and the sulfate flux experiments. The half-saturation constants for the chloride and the sulfate self-exchange amount to about 20 and 50 mM, respectively, and are consistent with the chloride and the sulfate half-saturation constants from the flux/concentration curves in the absence of NDS-TEMPO (Fig. 6).

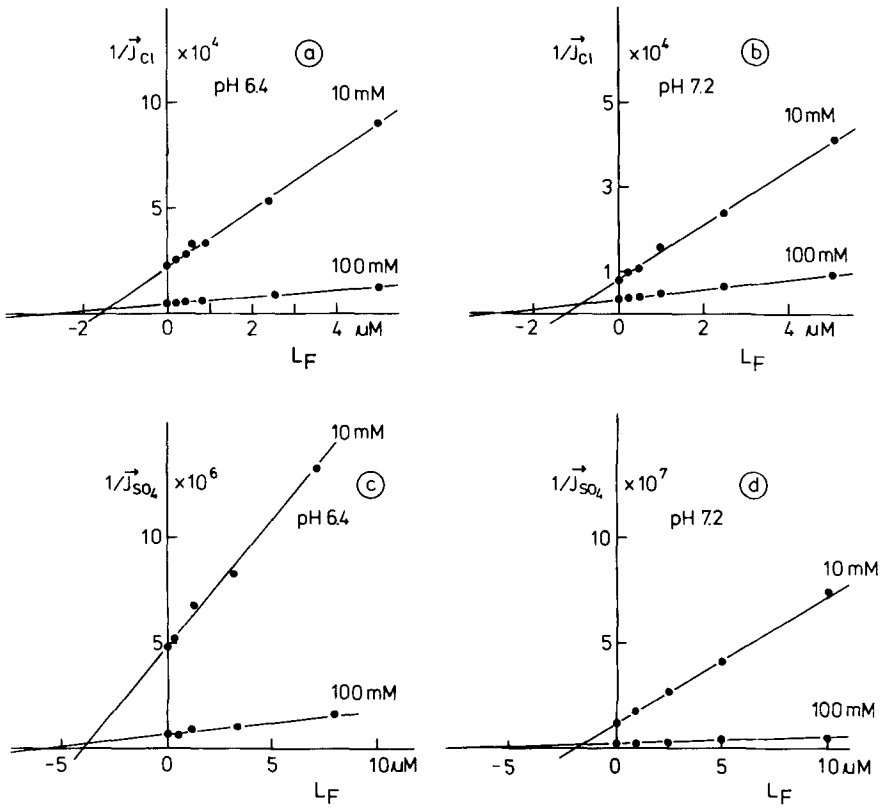

Fig. 7. Inhibition of chloride and of sulfate transport in human erythrocyte ghosts by NDS-TEMPO at different pH. Ordinate: (*a*, *b*) $1/\vec{J}_{Cl}$, (*c*, *d*) $1/\vec{J}_{SO_4}$ (mol/(min · g cells))$^{-1}$ reciprocal unidirectional flux of chloride or of sulfate, respectively. Abscissa: L_f (µM), concentration of free NDS-TEMPO in the incubation solution. The sulfate flux experiments were conducted at 25°C with 10% suspensions of erythrocyte ghosts, the chloride flux experiments were performed with 1% suspensions of erythrocyte ghosts at 0°C. pH, sulfate and chloride concentrations as indicated in the figure. Isosmotic substitution to 330 mosM by K-citrate

Table 4. pH Dependence of the inhibition of the chloride and the sulfate transport by NDS-TEMPO in resealed human erythrocyte ghosts[a]

pH	$K_{iL(app)}$ (µM)	K_{iL} (µM)	$K_{m(app)}$ (mM)	K_m (mM)
Chloride: 1% suspension of erythrocyte ghosts (0°C)				
6.4	1.35 ± 0.25	0.55 ± 0.12	62 ± 11	23 ± 4
7.2	0.75 ± 0.15	0.56 ± 0.13	29 ± 5	21 ± 4
8.0	0.55 ± 0.10	0.55 ± 0.10	19 ± 3	17 ± 3
Sulfate: 10% suspension of erythrocyte ghosts (25°C)				
6.4	3.65 ± 0.52	1.81 ± 0.37	147 ± 25	46 ± 9
7.2	2.15 ± 0.45	1.72 ± 0.32	70 ± 16	49 ± 14
8.0	1.92 ± 0.35	1.82 ± 0.5	39 ± 8	37 ± 8

[a] $K_{iL(app)}$ and $K_{m(app)}$ are the inhibition constant of NDS-TEMPO and the half-saturation constant of the substrate anion from the Dixon plots. K_{iL} and K_m are the NDS-TEMPO inhibition constant and half-saturation constant of the substrate anion corrected by the inhibition of NDS-TEMPO and substrate-anion binding by citrate^{2-}. K_{i2} of 40 mM for the chloride flux and of 70 mM for the sulfate flux experiments has been used. (*See* Fig. 8, plotting procedures.) Concentration of the suspension, temperature and pH as indicated in the table.

In order to correct for the effects of K-citrate, $K_{L(app)}$ and $K_{iL(app)}$ were replotted against I_{o2} (Table 2, Eqs. 44.1 and 48.1) while $K_{S(app)}$ and $K_{m(app)}$ were replotted against $(1 + K_{s(app)}/S_o)I_{o2}$ and $(1 + K_{m(app)}/S_o)I_{o2}$ (Table 2, Eqs. 49 and 50). I_{o2} is the concentration of divalent citrate at K-citrate substitution which is a function of pH. As shown in Fig. 8, the replots of $K_{L(app)}$ and of $K_{iL(app)}$ versus I_{o2} are linear except for the $K_{L(app)}$ value at pH 9.0. The replots of $K_{s(app/Cl)}$ versus $(1 + K_{s(app)}/S_o)I_{o2}$ and the replots of $K_{m(app/Cl)}$ and $K_{m(app/SO_4)}$ against $(1 + K_{m(app)}/S_o)I_{o2}$ were also linear, but the replots of $K_{s(app/SO_4)}$ versus $(1 + K_{s(app)}/S_o)I_{o2}$ were curved. The $K_{s(app/SO_4)}$ replots have not been shown. The linearity of the replots indicates that from pH 6.0 to 8.0, NDS-TEMPO binding and chloride binding are independent of pH while sulfate binding exhibits a strong pH dependency. The apparent substrate-site dissociation constant and the inhibition constants of NDS-TEMPO from the replots amount to approximately 1.3 µM, 0.5 µM from the chloride and 1.8 µM from the sulfate flux experiments (Fig. 8*a* and *b*), and agree fairly well. The chloride/substrate-site dissociation constant from the NDS-TEMPO binding studies is approximately 18 mM, the chloride and the sulfate half-saturation constants are approximately 17 and 35 mM (Fig. 8*c* and *d*). The inhibition constants for divalent citrate from the intersection of the straight lines with the abscissa range from 40 to 70 mM.

The close accordance of the NDS-TEMPO and the chloride-substrate-site dissociation constants from the NDS-TEMPO binding studies with the

NDS-TEMPO inhibition constant and the chloride half-saturation constant from the flux measurements provide strong evidence for the assumption that NDS-TEMPO binds to the substrate site of the Band 3 transport domain. At pH 7.2, the sulfate/substrate-site dissociation constant from NDS-TEMPO binding and the sulfate half-saturation constant from the flux measurements agree fairly well, but the sulfate/substrate-site dissociation constant and the sulfate half-saturation constant exhibit different patterns of pH responsiveness. The reasons for these discrepancies will be discussed below.

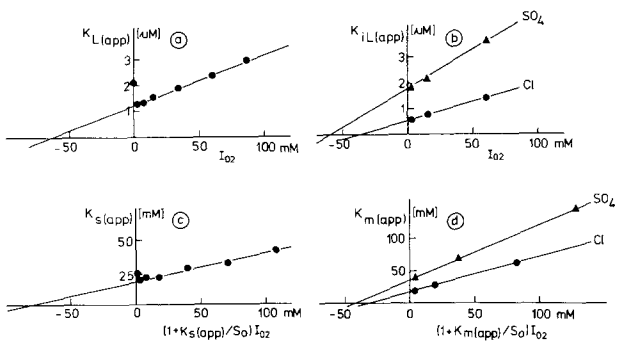

Fig. 8. Correction of NDS-TEMPO binding, chloride and sulfate binding to red cell ghosts for the inhibition by citrate^{2-}. (*a*, *b*) Replots of $K_{L(app)}$ and of $K_{iL(app)}$ versus I_{o2} (Table 2, Eqs. 44.1, 48.1). (*c*) Replot of $K_{s(app)}$ versus $(1 + K_{s(app)}/S_o)I_{o2}$ for chloride and of (*d*) $K_{m(app)}$ versus $(1 + K_{m(app)}/S_o)I_{o2}$ (Table 2, Eqs. 49 and 50). $K_{L(app)}$ and $K_{iL(app)}$ are the NDS-TEMPO/substrate-site dissociation and the NDS-TEMPO inhibition constant at zero substrate anion concentration, $K_{s(app)}$ and $K_{m(app)}$ are the anion/substrate-site dissociation constant and the half-saturation constant of the substrate anion, I_{o2} is the concentration of citrate^{2-} and S_o the concentration of an isotonic solution of the substrate anion. I_{o2} was calculated from the total citrate concentration and the pH of the solution. K_3, the dissociation constants for the 3rd dissociation step of citric acid is 6.4×10^{-7} M, 20°C (Handbook of Chemistry and Physics, 1982–1983). $K_{L(app)}$ and $K_{s(app)}$ refer to the NDS-TEMPO binding studies, $K_{iL(app)}$ and $K_{m(app)}$ to the flux measurements. The intercepts on the ordinate give the substrate-site dissociation constants for NDS-TEMPO and for the respective substrate anion corrected for the citrate^{2-} inhibition, the intersection points with the abscissa give K_{i2}, the substrate-site dissociation constant or the inhibition constant for citrate^{2-}. (For details *see* plotting procedures.)

Discussion

Anion transport across the erythrocyte membrane is mediated by a highly complex transport system. It is immediately evident that a transmembrane protein with a molecular weight of nearly 95,000 daltons cannot achieve translocation of the substrate anion by rotating across the membrane. By proteolytic cleavage, Band 3 can be split into an approximately 55,000 D "membrane domain" and an approximately 40,000 D "cytoplasmic domain." The Band 3 membrane domain catalyzes the anion transport, while the function of the cytoplasmic domain of Band 3 is not yet known (Jennings & Passow, 1979; Ramjeesingh et al., 1980; Rothstein, 1982; Jennings et al., 1984). Studies on the primary structure and the membrane orientation of Band 3 provide evidence that the polypeptide chain of the Band 3 membrane domain constitutes several membrane-spanning helices (Kopito & Lodish, 1985). These helices could form a channel of appropriate size and charge that catalyzes anion transport across the red cell membrane. A negatively charged residue could act as an "anionic gate" which controls the access of substrate anions to the channel at either side of the membrane. For these conditions, a channel could exhibit a typical carrier transport kinetics. Near the outer orifice of the channel, lysine, arginine, aspartate and glutamate residues have been localized by inhibitor binding studies which could participate in substrate-anion binding and serve as a sort of gate. (For details *see* Knauf, 1979, Macara & Cantley, 1983 and Passow, 1985.) ESR spectroscopy with NDS-TEMPO, a specific disulfonatostilbene spin label, offers the possibility of securing direct information on the interaction of the spin probe with the outer substrate site of the membrane domain of Band 3.

There are several lines of evidence which strongly suggest that NDS-TEMPO binds to the substrate site of Band 3. First, a mutual competition between substrate anion binding and NDS-TEMPO has been observed. Second, FDNB and DIDS, which bind preferentially to Band 3 and which are irreversible inhibitors of the anion transport in red blood cells, completely prevent the NDS-TEMPO binding to the erythrocyte membrane. Third, the addition of DIDS or of DNDS to NDS-TEMPO-labeled red blood cells results in an immediate release of bound NDS-TEMPO from the membrane surface, a disappearance of the immobile signal and a concomitant increase of the mobile ESR signal (Schnell et al., 1983).

Membrane-bound NDS-TEMPO appears to be almost completely immobilized. Upon subtraction of the mobile component, the ESR spectra display the features of a rigid powder spectrum. The immobilization could be accomplished either by the disulfonatostilbene moiety of the NDS-TEMPO sticking in a protein pocket or by a tight adsorption of NDS-TEMPO to the substrate site of Band 3, which is readily accessible from the outer but not from the inner membrane surface. The fact, that neither the shape of the immobile signal nor the number of NDS-TEMPO binding sites is affected by pH suggests that the protonation of the substrate site does not change from pH 6.0 to 8.0 and that the proton

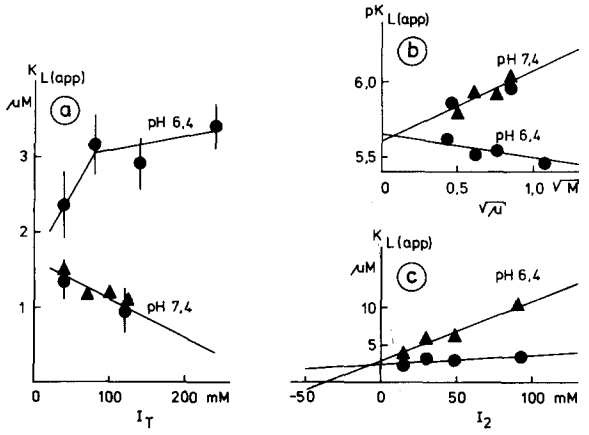

Fig. 9. Effects of K-citrate on NDS-TEMPO binding in resealed erythrocyte ghosts. (*a*) $K_{L(app)}$ against I_T, (●) without isosmotic substitution (mean ± SD, 4 expts), (▲) sorbitol substitution to 330 mosM (mean, 2 expts) (*b*) $pK_{L(app)}$ versus $\sqrt{\mu}$, same data as shown in *a*. (*c*) (●) $K_{L(app)}$ versus I_2, (▲) $K_{L(app)} \cdot 10^{\alpha\sqrt{\mu}}$ against I_2, data from *a*, pH 6.4. $\alpha = 0.4$ from *b*, pH 7.4. $K_{L(app)}$ denotes the NDS-TEMPO/substrate-site dissociation constant, I_2 and I_T are the concentration of divalent citrate and the total citrate concentration, μ is the ionic strength. 50% suspension of resealed erythrocyte ghosts, pH as indicated in the figure 20°C. I_2 calculated according to Eq. (36). For plot *b* the logarithmic form of Eq. (52) was used:

$$pK_{L(app)} = pK_{Lo} + \alpha\sqrt{\mu} - \log(1 + I_2/K_{i2}).$$

For plot *c* ▲ Eq. (52) was transformed to:

$$K_{L(app)}\, 10^{\alpha\sqrt{\mu}} = K_{Lo}(1 + I_2/K_{i2})$$

binding sites which regulate the transport process are not directly involved in NDS-TEMPO binding. Alternatively, NDS-TEMPO could prevent the binding of protons to the substrate site. To date we have no evidence for the latter supposition.

All experiments were executed with resealed red cell ghosts at self-exchange conditions. For the resealing of the erythrocyte ghosts, 40 mM K-citrate are required. In most of our experiments isosmotic substitution was made with 122 mM K-citrate. Although K-citrate does not penetrate the erythrocyte membrane, it is not an ideal substitute. Below pH 7.0, K-citrate has a weak inhibitory effect on chloride and on sulfate transport which increases as pH is reduced (Milanick & Gunn, 1982; Schnell & Besl, 1984; Hautmann & Schnell, 1985; Dobler & Schnell, *unpublished results*). Similarly, the NDS-TEMPO/substrate-site dissociation constants and the chloride/substrate-site dissociation constants increase at decreasing pH (Table 3). These results suggest that citrate^{2-} acts as a competitive inhibitor of NDS-TEMPO and of chloride binding in red cell ghosts, whereas citrate^{3-} appears to be ineffective. Other substitutes such as sucrose, sorbitol and Na-gluconate have been tested, but the NDS-TEMPO/substrate-site dissociation constants in 122 mM K-citrate were always lower than in isotonic K-citrate/sucrose, K-citrate/sorbitol or K-citrate/Na-gluconate solutions. Therefore most of the experiments have been executed in K-citrate solutions.

K-citrate exerts a duplicate effect upon NDS-TEMPO binding. The addition of K-citrate to the solution results in an increase of ionic strength which in turn elicits a salting-out effect upon NDS-TEMPO binding. On the other hand, divalent citrate acts as a competitive inhibitor of NDS-TEMPO binding. The salting-out effect tends to reduce the observed NDS-TEMPO/substrate-site dissociation constant while the competitive inhibition of NDS-TEMPO binding by divalent citrate tends to increase the observed NDS-TEMPO/substrate-site dissociation constant. At pH 7.4, the salting-out effect prevails and $K_{L(app)}$ decreases as the concentration of citrate is elevated. Conversely, at pH 6.4, the inhibitory effect of citrate^{2-} on NDS-TEMPO binding predominates and $K_{L(app)}$ increases as the K-citrate concentration is raised (Fig. 9*a*).

The binding of NDS-TEMPO to the substrate site involves electrostatic forces and hydrophobic interactions, and the overall effect of ionic strength is difficult to predict. Using the Debye-Hückel equation as an approximation, K_L is given by (*cf.* Webb, 1963)

$$K_L = K_{Lo} \cdot 10^{-\alpha\sqrt{\mu}}. \tag{51}$$

Substituting K_L from Eq. (51) into Eq. (43.1), Table 2, $K_{L(app)}$ can be written as

$$K_{L(app)} = K_{Lo} \cdot 10^{-\alpha\sqrt{\mu}}(1 + I_2/K_{i2}). \tag{52}$$

$K_{L(app)}$ is the NDS-TEMPO/substrate-site dissociation constant, K_L the NDS-TEMPO/substrate-site dissociation constant corrected for the inhibition by citrate^{2-}, and K_{Lo} the thermodynamic dissociation constant. $\mu = 0.5\Sigma c_i z_i^2$ is the ionic strength with c_i and z_i being the concentration and the valency of the i-th ion species, and α is an empirical constant. I_2 is the concentration of divalent citrate and K_{i2} is the citrate^{2-}/substrate-site dissociation constant. The effect of ionic strength upon the ionization of citrate has been disregarded.

The plots of $pK_{L(app)}$ against $\sqrt{\mu}$ are linear, but the slopes of the plots change with pH (Fig. 9*b*). At pH 7.4, α is approximately +0.4 while, at pH 6.4, α is about −0.2. On the other hand, the straight lines intersect the $pK_{L(app)}$ axis at approximately the same point. These results indicate that for both pH values the thermodynamic NDS-TEMPO/substrate-site dissociation constants are identical and rule out the possibility that the increase of $K_{L(app)}$ is caused by the binding of a proton to the substrate site. The

thermodynamic NDS-TEMPO/substrate-site dissociation constant amounts to approximately 2.5 μM.

Figure 9*c* shows the inhibitory effect of citrate^{2-} on NDS-TEMPO binding. At pH 6.4, $K_{L(app)}$ increases as the concentration of citrate^{2-} is raised, but the replots of $K_{L(app)}$ versus I_2 were always curved (Fig. 9*c*, circles). Upon correction for the effects of ionic strength, the replot of $K_{L(app)}$ versus I_2 is linear and provides a K_{i2} value of about 40 mM (Fig. 9*c*, triangles). This value is consistent with the K_{i2} values from the K-citrate substitution experiments (Fig. 8).

The NDS-TEMPO binding data and the flux measurements can best be analyzed by appropriate plotting procedures. Because of the low specificity of the substrate site, K-citrate cannot be replaced by an "inert salt" which would not interfere with NDS-TEMPO or substrate-anion binding. However, we can eliminate the effects of the substitute anion by an appropriate analysis of the data. As outlined above, NDS-TEMPO binding to the Band 3 substrate site follows a simple adsorption equilibrium. The number of NDS-TEMPO binding sites per cell is always obtained from the maximum NDS-TEMPO binding capacity of the suspension and the number of cells, irrespective of whether or not the substitute anion acts as a competitive inhibitor. However, the effects of pH on the affinity of NDS-TEMPO and substrate anions to the substrate site may be obscured by the presence of an ionizing, competitive inhibitor. The effects of citrate^{2-} can be assessed by replots as shown in Fig. 8.

The pH dependence of NDS-TEMPO binding to resealed erythrocyte ghosts is summarized in Fig. 10. The maximum number of NDS-TEMPO binding sites per cell is approximately 1.0×10^6 and appears to be independent of pH. The number of NDS-TEMPO binding sites per erythrocyte is consistent with the number of H_2-DIDS binding sites (Lepke et al., 1976) and of DNDS binding sites (Fröhlich, 1982). The NDS-TEMPO/substrate-site and the chloride/substrate-site dissociation constant corrected for the inhibition by citrate^{2-} are almost independent of pH and amount to ~1.3 μM and to ~17 mM. Above pH 8.0, both constants show a slight increase. The NDS-TEMPO/substrate-site dissociation constant from the NDS-TEMPO binding studies agrees fairly well with the NDS-TEMPO inhibition constants from the sulfate and the chloride flux measurements which amount to 1.8 and to 0.5 μM (Table 4). The chloride/substrate-site dissociation constant from the NDS-TEMPO binding studies are in accordance with the chloride half-saturation constants from the Dixon plots (Table 4) and the chloride half-saturation constants from the flux/concentration curves (Fig. 6).

The chloride half-saturation constants amount to approximately 20 mM and display the same pattern of pH response as the substrate-site dissociation constant of chloride from the ESR spectroscopy. By contrast, the substrate-site dissociation constant and the half-saturation constant of sulfate exhibit different patterns of pH response. At pH 7.2, both constants amount to approximately 50 mM, but the substrate-site dissociation constant of sulfate decreases as pH is reduced (Fig. 10) while the sulfate half-saturation constant remains constant (Fig. 6). The replots of $K_{s(SO_4)}$ versus 1/H from the lower branch of the $K_{s(SO_4)}$/pH curves yielded a sulfate dissociation constant of about 2 mM and a pK in the range of 5.3 to 5.6 for the group that participates in sulfate binding.

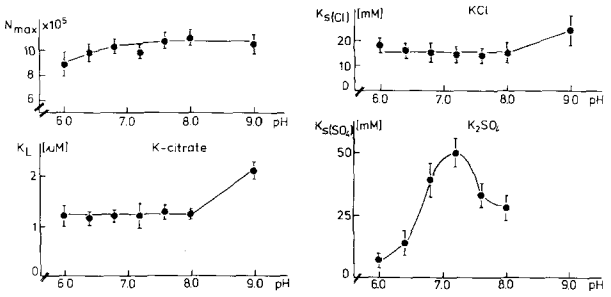

Fig. 10. pH dependence of NDS-TEMPO binding of chloride and of sulfate binding to human erythrocyte ghosts. N_{max} is the maximal number of NDS-TEMPO binding sites/cell, K_L is the NDS-TEMPO substrate-site dissociation constant corrected for citrate^{2-} inhibition, $K_{s(Cl)}$ and $K_{s(SO_4)}$ are the substrate-site dissociation constants of chloride and of sulfate corrected for citrate^{2-} inhibition. The respective K_{i2} values for the correction of $K_{L(app)}$, $K_{s(app/Cl)}$ and $K_{s(app/SO_4)}$, $K_{iL(app/SO_4)}$ and $K_{m(app/SO_4)}$ are in the range of 60 to 70 mM, the K_{i2} values for the correction of $K_{iL(app/Cl)}$ and $K_{m(app/Cl)}$ (0°C) are in the range of 30 to 40 mM. *Compare* Fig. 8

Concerning the pH dependence of chloride and of sulfate transport in erythrocyte ghosts, our results are in accordance with previous studies in red cells. Sulfate and phosphate self-exchange display a pH optimum at about pH 6.4 (Deuticke, 1970; Schnell, 1972; Schnell et al., 1981*a*). At 0°C, the chloride self-exchange in intact red cells exhibits pH maxima at about pH 7.5 which disappear at high chloride concentrations (Gunn et al., 1973; Wieth et al., 1973; Dalmark, 1975, 1976; Wieth & Bjerrum, 1982; Wieth et al., 1982).

The pH dependence of the maximal unidirectional chloride and sulfate fluxes and the pH dependence of the chloride and the sulfate half-saturation constants in erythrocyte ghosts have not been studied in detail. Within the pH range of 6.0 to 8.0, the apparent half-saturation constants of chloride and of sulfate are almost independent of pH, while the maximal unidirectional fluxes exhibit a clear pH dependency with pH maxima at about 6.4 and 7.6 (Fig. 6). Above pH 8.0, an increase of the chloride and of the sulfate half-saturation constants has been

observed. In these experiments isosmotic substitution has been made by sorbitol or sucrose and the citrate concentration is low. Therefore no corrections for divalent citrate have been made. A crude estimate of the error can be made by substituting the inhibition constants of citrate^{2-} from the K-citrate substituting experiments (Fig. 8*b*). The apparent chloride half-saturation constant at pH 6.2 would be approximately 20% smaller whereas the apparent sulfate half-saturation constant would be approximately 15% smaller than the respective half-saturation constant at pH 7.2. Above pH 7.0, the citrate^{2-} inhibition is negligible. The presence of a fixed concentration of K-citrate has no effect on the maximal unidirectional fluxes of sulfate and of chloride.

Milanick and Gunn (1982) found a decrease of the sulfate inhibition constant with decreasing pH and a random-ordered type of sulfate and of proton binding. The sulfate inhibition constant from the chloride flux measurements corrected for proton binding was 4.35 ± 0.56 mM and the pK of the proton binding site in the absence of sulfate was 5.03 ± 0.2. From a qualitative point of view, the results of Milanick and Gunn (1982) are consistent with the results from our NDS-TEMPO binding studies except that their sulfate inhibition constants from the chloride flux measurements are lower than the sulfate/substrate-site dissociation constant from our NDS-TEMPO binding studies. Possibly, these differences arise from the different temperature at which the experiments have been conducted.

Throughout the pH range of 6.0 to 9.0, a competitive inhibition of NDS-TEMPO binding by chloride and sulfate and a competitive inhibition of chloride and of sulfate binding by NDS-TEMPO was observed. The mutual competition between NDS-TEMPO, chloride and sulfate, and the close accordance of the NDS-TEMPO/substrate-site dissociation constant with the NDS-TEMPO inhibition constants indicates that NDS-TEMPO binds to the substrate site of Band 3. The strong pH dependence of the maximal unidirectional fluxes of chloride and of sulfate, on the other hand, contrasts with the pH insensitivity of NDS-TEMPO binding. In addition, the differences between chloride binding and sulfate binding are not yet understood.

The simple diprotic anion-transport model shown in Fig. 2 may exhibit a number of quite unexpected transport phenomena. Depending upon the relative magnitudes of the translocation rates, it may display a substrate-anion/proton cotransport, a substrate-anion/proton countertransport, a tightly coupled anion exchange or a simple proton transport. The pH dependence of the chloride, the sulfate and the phosphate transport indicates that several ionizable groups participate in the regulation of anion transport across the red cell membrane. These ionizable groups can be involved in substrate-anion binding, in transport catalysis or in both of these effects. The ionizable groups outside the substrate site were designated as being regulator sites. These regulator sites could activate or inhibit the conformational changes of the Band 3 transport domain, which is associated with substrate-anion translocation, without having any effect upon substrate-anion binding. If the ionization of the regulator sites has no effect upon NDS-TEMPO and substrate-anion binding, the maximum number of NDS-TEMPO binding sites is independent of pH while the maximal unidirectional fluxes of the substrate anions could display a strong pH responsiveness. The NDS-TEMPO/substrate-site dissociation constant and the half-saturation constant of the substrate anion, on the other hand, should be independent of pH (Table 1). These predictions are in accordance with our experimental results.

The different pH dependence of the chloride/substrate-site and the sulfate/substrate-site dissociation constant could indicate a partial overlap of the chloride and the sulfate binding site. For sulfate binding, when two negative charges are introduced into the substrate site, an additional prototropic group seems to be involved. This group is positioned at the substrate site or in its immediate vicinity and could account for the pH dependence of the sulfate/substrate-site dissociation constant. The binding of an additional proton could counterbalance the negative excess charge and could improve the conditions for conformational changes of the Band 3 transport domain by reducing electrostatic repulsion forces.

The mutual competition between NDS-TEMPO, chloride and sulfate binding indicates that NDS-TEMPO binds to the substrate site of the Band 3 transport domain. The sulfonyl groups of NDS-TEMPO could interact with ionizable groups of the substrate site. Changes of the ionization of these groups should elicit changes of the mobility of bound NDS-TEMPO or changes of its affinity to the substrate site. However, none of these effects has been observed. Thus we are forced to the conclusion that the regulator sites, which are responsible for the pH dependence of the substrate-anion transport, are positioned outside the substrate site of the Band 3 transport domain.

This paper was supported by The Deutsche Forschungsgemeinschaft. We are indebted to Prof. Dr. C. Albers, Prof. Dr. A. Müller-Broich, and Prof. Dr. J. Sauer for their support of our work. We thank Dr. Mertens, Bayer AG., Leverkusen, for sup-

plying ANDS. We wish to thank, in particular, Dr. R. Knopp and Dr. E. Eibler for their helpful suggestion concerning the recording of the ESR spectra and the HPLC runs. We wish to express our thanks to Mrs. E. Besl and Mrs. A. Stangl for expert technical assistance and Mrs. H. Trommer for patient typewriting of the manuscript.

References

Berghout, A., Raida, M., Romano, L., Passow, H. 1985. pH-dependence of phosphate transport across the red blood cell membrane after modification by dansyl chloride. *Biochim. Biophys. Acta* **815**:281–286

Bodemann, H., Passow, H. 1972. Factors controlling the resealing of the membrane of human erythrocyte ghosts after hypotonic hemolysis. *J. Membrane Biol.* **8**:1–26

Brahm, J. 1977. Temperature-dependence of chloride transport kinetics in human red blood cells. *J. Gen. Physiol.* **70**:283–306

Cabantchik, Z.I., Rothstein, A. 1972. The nature of the membrane sites controlling anion permeability of human red blood cells as determined by studies with disulfonic stilbene derivatives. *J. Membrane Biol.* **10**:311–330

Cabantchik, Z.I., Rothstein, A. 1974. Membrane proteins related to anion permeability of human red blood cells. I. Localization of disulfonic stilbene binding sites in proteins involved in permeation. *J. Membrane Biol.* **15**:207–226

Dalmark, M. 1975. Chloride transport in human red cells. *J. Physiol. (London)* **250**:39–64

Dalmark, M. 1976. Chloride in the human erythrocyte: Distribution and transport between cellular and extracellular fluids and structural features of the cell membrane. *Prog. Biophys. Mol. Biol.* **31**:145–164

Dalmark, M., Wieth, J.O. 1972. Temperature dependence of chloride, bromide, iodide, thiocyanate and salicylate transport in human red cells. *J. Physiol. (London)* **224**:583–610

Deuticke, B. 1970. Anion permeability of the red blood cell. *Naturwissenschaften* **57**:172–179

Dix, J.A., Verkan, A.S., Solomon, A.K., Cantley, L.C. 1979. Human erythrocyte anion exchange site characterized using a fluorescence probe. *Nature (London)* **282**:520–522

Fröhlich, O. 1982. The external anion binding site of the human erythrocyte anion transporter: DNDS binding and competition with chloride. *J. Membrane Biol.* **65**:111–123

Furuya, W., Tanya, T., Law, F.Y., Knauf, P.A. 1984. Transmembrane effects of intracellular chloride on the inhibitory potency of extracellular H_2DIDS. Evidence for two confirmations of the transport site of the human erythrocyte anion exchange protein. *J. Gen. Physiol.* **83**:657–681

Gardos, G., Hoffmann, J.F., Passow, H. 1969. Flux measurements in erythrocytes. *In:* Laboratory Techniques in Membrane Biophysics. H. Passow and R. Stämpfli, editors. pp. 9–20. Springer, Berlin-Heidelberg-New York

Gunn, R.B., Dalmark, M., Tosteson, D., Wieth, J.O. 1973. Characteristics of chloride transport in human red blood cells. *J. Gen. Physiol.* **61**:185–206

Hautmann, M., Schnell, K.F. 1985. Concentration dependence of the chloride selfexchange and homoexchange fluxes in human red cell ghosts. *Pfluegers Arch.* **405**:193–201

Heinz, E. 1978. Mechanics and Energetics of Biological Transport. Springer, Berlin-Heidelberg-New York

Jennings, M.L. 1976. Proton fluxes associated with erythrocyte membrane anion exchange. *J. Membrane Biol.* **28**:187–205

Jennings, M.L. 1980. Apparent recruitment of SO_4 transport sites by the Cl gradient across the human erythrocyte membrane. *In:* Membrane Transport in Erythrocytes. U.V. Lassen, H.H. Ussing, and J.O. Wieth, editors. Alfred Benzon Symposium 14. pp. 450–463. Munksgaard, Copenhagen

Jennings, M.L. 1985. Kinetics and mechanism of anion transport in red blood cells. *Annu. Rev. Physiol.* **47**:519–533

Jennings, M.L., Passow, H. 1979. Anion transport across the erythrocyte membrane, in situ proteolysis of band 3 protein, and cross-linking of fragments by 4,4′-diisothiocyano-dihydrostilbene-2,2′-disulfonate. *Biochim. Biophys. Acta* **55**:498–519

Jost, P., Griffith, O.H. 1976. Instrumental aspects of spin labeling. *In:* Spin Labeling, Theory and Application. L.J. Berliner, editor. pp. 251–272. Academic, New York

Knauf, P.A. 1979. Erythrocyte anion exchange and the band 3 protein: Transport kinetics and molecular structure. *Curr. Top. Membr. Transp.* **12**:249–363

Knauf, P.A., Law, F.Y., Tarshis, T., Furuya, W. 1984. Effects of the transport site conformation on the binding of external NAP-taurine to the human erythrocyte anion exchange system. Evidence for intrinsic asymmetry. *J. Gen. Physiol.* **83**:683–701

Kopito, R.R., Lodish, H.F. 1985. Primary structure and transmembrane orientation of murine anion exchange protein. *Nature (London)* **316**:234–238

Kotyk, A., Janácek, K. 1970. Cell Membrane Transport: Principles and Techniques. Plenum, New York-London

Lepke, S., Fasold, H., Pring, M., Passow, H. 1976. A study of the relationship between inhibition of anion exchange and binding to the red blood cell membrane of 4,4′-diisothiocyano stilbene-2,2′-disulfonic acid (DIDS) and its dihydro derivative (H_2DIDS). *J. Membrane Biol.* **29**:147–177

Lepke, S., Passow, H. 1972. The effect of pH at hemolysis on the reconstitution of low cation permeability in human erythrocyte ghosts. *Biochim. Biophys. Acta* **255**:696–702

Macara, I.G., Cantley, L.C. 1983. The structure and function of band 3. *In:* Cell Membranes: Methods and Reviews. E. Elson, W. Frazier, and L. Glaser, editors. Vol. 1, pp. 41–87. Plenum, New York

Marsh, D. 1981. Electron spin resonance: Spin labels. *In:* Membrane Spectroscopy. E. Grell, editor. pp. 51–142. Springer, Berlin-New York

Milanick, M.A., Gunn, R.B. 1982. Proton-sulfate co-transport. Mechanism of H^+ and sulfate addition to the transporter of human red blood cells. *J. Gen. Physiol.* **79**:87–113

Passow, H. 1969. Passive ion permeability of the erythrocyte membrane. *Prog. Biophys. Mol. Biol.* **19**:424–467

Passow, H. 1982. Anion-transport-related conformational changes of the band 3 protein in the red blood cell membrane. *In:* Membranes and Transport. A.N. Martonosi, editor. Vol. 2, pp. 451–460. Plenum, New York-London

Passow, H. 1985. Molecular aspects of band 3 protein mediated anion transport across the red blood cell membrane. *Rev. Physiol. Biochem. Pharmacol.* **103** (*in press*)

Ramjeesingh, M., Grinstein, S., Rothstein, A. 1980. Intrinsic segments of band 3 that are associated with anion transport across red blood cell membranes. *J. Membrane Biol.* **57**:95–102

Rao, A., Martin, P., Reithmeier, R.A.F., Cantley, L.C. 1979. Location of the stilbene disulfonatostilbene binding site of the human erythrocyte anion-exchange system by resonance energy transfer. *Biochemistry* **18**:4505–4516

Rothstein, A. 1982. Functional structure of band 3, the anion

transport protein of the red blood cells, as determined by proteolytic and chemical cleavages. *In:* Membranes and Transport. A.N. Martonosi, editor. Vol. 2, pp. 435–440. Plenum, New York

Schnell, K.F. 1972. On the mechanism of inhibition of the sulfate transfer across the human erythrocyte membrane. *Biochim. Biophys. Acta* **282:**265–276

Schnell, K.F. 1977. Anion transport across the red blood cell membrane mediated by dielectric pores. *J. Membrane Biol.* **37:**99–136

Schnell, K.F. 1979. The anion transport system of the red blood cell. *In:* Biophysics of Membrane Transport. J. Kuczera, J. Gabrielska, and S. Przestalski, editors. pp. 216–252. Dept. of Agriculture, University of Wroslaw

Schnell, K.F., Besl, E. 1984. Concentration dependence of the unidirectional sulfate and phosphate flux in human red cell ghosts under self-exchange and under homoexchange conditions. *Pfluegers Arch.* **402:**197–206

Schnell, K.F., Besl, E., Manz, A. 1978. Asymmetry of the chloride transport system in human erythrocyte ghosts. *Pfluegers Arch.* **375:**87–95

Schnell, K.F., Besl, E., Mosel, R.v. der 1981*a*. Phosphate transport in human red blood cells: Concentration dependence and pH dependence of the unidirectional phosphate flux at equilibrium conditions. *J. Membrane Biol.* **61:**173–192

Schnell, K.F., Elbe, W., Käsbauer, J., Kaufmann, E. 1983. Electron spin resonance studies of the inorganic-anion-transport system of the human red blood cell. Binding of a disulfonatostilbene spin label (NDS-TEMPO) and inhibition of anion transport. *Biochim. Biophys. Acta* **732:**226–275

Schnell, K.F., Gerhardt, S. 1973. The effect of the membrane potential on the anion exchange across the erythrocyte membrane. *Pfluegers Arch.* **343:**R60

Schnell, K.F., Gerhardt, S., Schöppe-Fredenburg, A. 1977. Kinetic characteristics of the sulfate self-exchange in human red blood cells and red blood cell ghosts. *J. Membrane Biol.* **30:**319–350

Schnell, K.F., Käsbauer, J., Kaufmann, E. 1981*b*. ESR-studies on the anion transport system of the human red blood cell: Evidence for conformational changes related to the transport function. *Pfluegers Arch.* **391:**R21

Schnell, K.F., Käsbauer, J., Kaufmann, E., Elbe, W. 1981*c*. ESR-affinity labeling of the inorganic anion transport system of the human red blood cell. *Pfluegers Arch.* **389:**R47

Segel, I.H. 1975. Enzyme kinetics, behavior and analysis of rapid equilibrium and steady-state enzyme systems. John Wiley and Sons, New York-London-Sidney-Toronto

Ship, S., Shami, Y., Breuer, W., Rothstein, A. 1977. Synthesis of tritiated 4,4′-diisothiocyano-2,2′-stilbene disulfonic acid ([^{3}H]DIDS) and its covalent reaction with sites related to anion transport in human red blood cells. *J. Membrane Biol.* **33:**311–324

Weast, R.C., Melvin, J.A. 1982–1983. Handbook of Chemistry and Physics, 63rd edition. CRC Press, Boca Raton, Florida

Webb, J.L. 1963. Enzyme and Metabolic Inhibitors, Vol. I. Academic, New York-London

Wieth, J.O., Bjerrum, P. 1982. Titration of transport and modifier sites in the red cell anion transport system. *J. Gen. Physiol.* **79:**253–282

Wieth, J.O., Andersen, O.S., Brahm, J., Bjerrum, P.J., Borders, C.L. 1982. Chloride-bicarbonate exchange in red blood cells: Physiology of transport and chemical modification of binding sites. *Phil. Trans. R. Soc. London B* **299:**383–399

Wieth, J.O., Dalmark, M., Gunn, R.B., Tosteson, D.C. 1973. The transfer of monovalent inorganic anion through the red cell membrane. *In:* Erythrocytes, Thrombocytes, Leukocytes. E. Gerlach, K. Moser, E. Deutsch, and W. Wilmans, editors. pp. 71–76. Thieme, Stuttgart

Wood, P.G., Passow, H. 1981. Techniques for the modification of the intracellular composition of red blood cells. *In:* Techniques in Cellular Physiology. p. 112. Elsevier/North-Holland Scientific, Amsterdam

Zaki, L., Fasold, H., Schuhmann, B., Passow, H. 1975. Chemical modification of membrane proteins in relation to the inhibition of anion exchange in human red blood cells. *J. Cell. Physiol.* **86:**471–494

Received 22 July 1985; revised 23 December 1985